

Catastrophic Overfitting: A Potential Blessing in Disguise

Mengnan Zhao, Lihe Zhang,* Yuqiu Kong, Baocai Yin

Abstract

Fast Adversarial Training (FAT) has gained increasing attention within the research community owing to its efficacy in improving adversarial robustness. Particularly noteworthy is the challenge posed by catastrophic overfitting (CO) in this field. Although existing FAT approaches have made strides in mitigating CO, the ascent of adversarial robustness occurs with a non-negligible decline in classification accuracy on clean samples. To tackle this issue, we initially employ the feature activation differences between clean and adversarial examples to analyze the underlying causes of CO. Intriguingly, our findings reveal that CO can be attributed to the feature coverage induced by a few specific pathways. By intentionally manipulating feature activation differences in these pathways with well-designed regularization terms, we can effectively mitigate and induce CO, providing further evidence for this observation. Notably, models trained stably with these terms exhibit superior performance compared to prior FAT work. On this basis, we harness CO to achieve ‘attack obfuscation’, aiming to bolster model performance. Consequently, the models suffering from CO can attain optimal classification accuracy on both clean and adversarial data when adding random noise to inputs during evaluation. We also validate their robustness against transferred adversarial examples and the necessity of inducing CO to improve robustness. Hence, CO may not be a problem that has to be solved.

1. Introduction

In recent years, the realm of deep learning has witnessed remarkable advancements [28, 32, 50]. However, the widespread adoption of deep neural networks [3, 34] has inevitably prompted researchers to examine their limitations [6, 8, 40], particularly their vulnerability to adversarial attacks [4, 15, 49]. For improving model robustness, adversarial training [20, 27, 42] serves as a typical technique that incorporates perturbed samples into the training dataset. Nevertheless, conventional adversarial training approaches [16, 22, 43] bear the burden of time-intensive processes, *i.e.*,

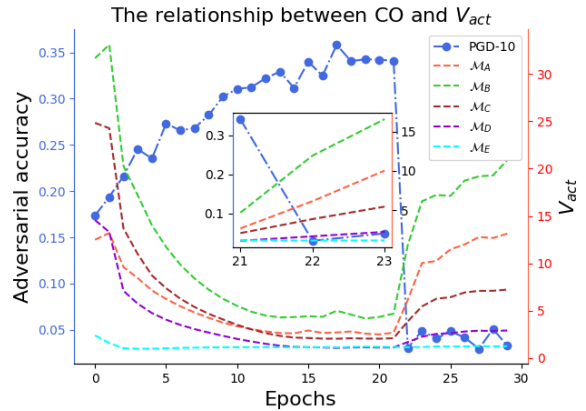


Figure 1. Relationship between catastrophic overfitting and feature activation differences V_{act} during adversarial training. We select CIFAR-10 [23] as the dataset and ResNet18 [17] as the network \mathcal{M} . Five activation nodes $\mathcal{M}_{A\sim E}$ are chosen from \mathcal{M} . Left y-axis: Model robustness against the PGD-10 attack; Right y-axis: V_{act} on various activation nodes. V_{act} is quantified using L_2 regularization between features of clean and adversarial examples.

generating adversarial training data using multi-step attacks such as the projected gradient descent (PGD) [26]. Therefore, researchers have progressively shifted their attention towards fast adversarial training (FAT) [21, 25, 47].

FAT methods commonly employ a one-step, fast gradient-sign method (FGSM) [14] to generate adversarial training data. While these approaches are more time-efficient than PGD-based adversarial training, they often face the challenge of catastrophic overfitting (CO) [10, 33], *i.e.*, the classification accuracy of trained models for adversarial examples encounters a sudden decrease. This challenge becomes increasingly prevalent as the perturbation budget ξ is expanded during adversarial training [48]. To solve it, researchers are dedicated to enhancing the diversity of adversarial perturbations [19, 41] and introducing additional regularization terms [2, 44]. Even though these advanced techniques exhibit notable progress in addressing the stability concern, their performance on clean samples significantly declines. For instance, ResNet18 [17] can achieve an impressive 94% classification accuracy on clean CIFAR-10 [23] samples, but the accuracy drops to 64% when $\xi = 16/255$ during adversarial training, as shown in [48]. This prompts us to explore CO in depth.

He et al. [18] think that the self-fitting results in CO

*Corresponding author

and utilize a high-variance channel masking approach to eliminate the attack information. However, the channels responsible for learning data information can also exhibit high variance, as demonstrated in our experiments. Therefore, we introduce a more effective channel-selecting method – feature activation differences between clean and adversarial examples, to provide a comprehensive explanation for CO. As depicted in Fig. 1, CO is accompanied by salient feature activation differences. By deliberately suppressing or enlarging feature activation differences of several specific channels using well-designed regularization terms, we can effectively address or induce CO, respectively. This actually further verifies the relationship between CO and salient feature differences. Notably, under stable adversarial training, the proposed regularization terms approach zero and are thus insensitive to the choice of hyperparameters.

On this basis, we try to improve the adversarial robustness of CO-affected models by leveraging CO, while maintaining their performance on clean samples. This can be realized by introducing processing techniques that possess threefold capacities: 1) preserve valuable data information; 2) disrupt potential attack information embedded in adversarial examples; 3) have timeliness. As a result, adding random noise to model inputs during evaluation is a simple yet effective manner. It helps CO-affected models realize optimal classification accuracy for both clean and adversarial data, and does not improve the performance of models exclusively trained on clean samples. We explain this phenomenon from a novel perspective of “attack obfuscation”.

The contributions are summarized as follows: **(1)** We systematically analyze the causes of CO by examining feature activation differences between clean and adversarial examples. These differences can more precisely identify the specific channels responsible for CO than previous studies; **(2)** We present novel regularization terms to avoid (or induce) CO by deliberately suppressing (or amplifying) feature activation differences in several selected channels. Models trained stably with these terms achieve better or comparable performance to state-of-the-art FAT techniques; **(3)** We leverage CO to enhance model performance. By applying random noise to model inputs during evaluation, CO-affected models attain optimal classification accuracy for both clean and adversarial examples. We analyze this phenomenon from the perspective of attack obfuscation and give full experimental evidence.

2. Related work

To improve the adversarial robustness of deep models, researchers commonly employ adversarial training techniques, *i.e.*, enhancing the training dataset D_{train} with adversarial perturbations (δ). A typical adversarial training

formula [26] tackles a min-max optimization problem,

$$\min_{\theta} \mathbb{E}_{(x,y) \sim D_{train}} \left[\max_{\delta \in [-\xi, \xi]} \mathcal{L}(\mathcal{M}(x + \delta), y) \right], \quad (1)$$

where $\mathcal{M}(\cdot)$ denotes a fixed victim model parameterized by θ . ξ describes the maximum perturbation budget. $\mathcal{L}(\cdot)$ is typically the cross-entropy loss. The internal maximization often yields un-targeted adversarial examples based on the original targets y of inputs x . An alternative adversarial training paradigm [37, 46] applies a regression constraint to clean samples and introduces regularization terms to align the predictions for clean x and adversarial examples $x + \delta$,

$$\min_{\theta} \mathbb{E}_{(x,y) \sim D_{train}} [\mathcal{L}(\mathcal{M}(x), y) + \|\mathcal{M}(x + \delta) - \mathcal{M}(x)\|_*], \quad (2)$$

where $\|\cdot\|_*$ signifies a norm function. δ in both Eqs. (1) and (2) is usually generated by the gradient-based adversarial attacks [30, 39, 45]. For instance, Goodfellow et al. [14] proposed a single-step gradient attack – FGSM,

$$\delta = \xi \cdot \text{sign}(\nabla_x \mathcal{L}(\mathcal{M}(x), y)), \quad (3)$$

where $\text{sign}(\cdot)$ is the sign function. $\nabla_x \mathcal{L}(\cdot)$ denotes the gradient backward. Similarly, Cheng et al. [7] introduced the fast gradient non-sign method, which incorporates a scale factor ζ to control ξ , $\zeta = \frac{\|\text{sign}(\delta)\|_2}{\|\delta\|_2}$. Apart from single-step attacks, there are also multi-step attacks [11, 24, 26] that employ a small stride ϵ and restrict the ξ at each step t ,

$$\begin{aligned} x'_{t+1} &= \text{clip}_{\xi}(x'_t + \epsilon \cdot \text{sign}(\nabla_{x'_t} \mathcal{L}(\mathcal{M}(x'_t), y))), \\ \delta &= x'_{final} - x. \end{aligned} \quad (4)$$

Based on the types of adversarial attacks, adversarial training techniques can be broadly categorized into two kinds, *i.e.*, fast adversarial training methods [21, 31, 35] utilizing single-step attacks like FGSM and conventional methods that rely on multi-step attacks [22, 38, 42] such as PGD. Compared to PGD-based methods, FGSM-based approaches require less time but are susceptible to CO. To mitigate CO, various techniques have been introduced, such as FGSM-RS [41], GradAlign [29], NuAT [37], ZeroGrad [12], and ConvergeSmooth [48]. However, the enhancement of adversarial robustness brought by these methods often decreases the classification accuracy on clean samples. Furthermore, increasing the perturbation budget during adversarial training will further reduce this accuracy.

Inspired by [18], we revisit CO. Surprisingly, we observe that by simply introducing random noise to inputs during evaluation, the CO-affected models can achieve excellent adversarial robustness while maintaining their classification accuracy on clean examples. This discovery challenges the conventional cognition and raises a question about whether CO is indeed a problem that requires to be solved.

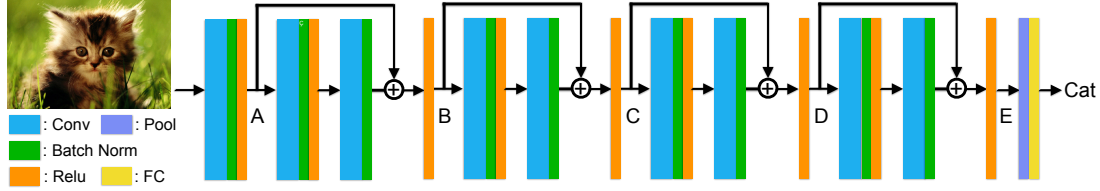


Figure 2. Overall architecture and the placement of activation nodes. We select five activation nodes in the network ResNet18, and each node locates after a ReLU function.

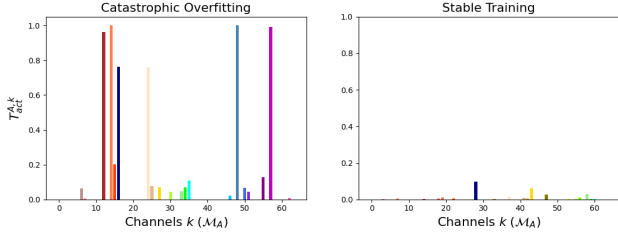


Figure 3. Statistical analyses of channel-specific feature activation differences at the activation node \mathcal{M}_A .

3. What causes catastrophic overfitting?

In this section, we investigate the causes of CO through experiments. For a fair comparison, we follow [44, 48] to realize the FAT baseline, FGSM-MEP [44]. The perturbation budget during adversarial training (ξ_T) is set to 12/255 to ensure the occurrence of CO. We expand the perturbation budget for evaluation (ξ_E) to 16/255 as the uncertainty perturbation degree of attacks. The larger values of ξ_E are not considered since they may change human predictions [1].

3.1. Relationship between CO and V_{act}

Prior work [18] believes that high-variance feature channels are responsible for CO. However, we find that masking these channels greatly affect the classification accuracy on clean samples, as shown in Fig. 4. Therefore, we introduce the feature activation differences to more precisely determine the channels closely associated with CO.

Taking ResNet18 as an example, five activation nodes are selected, with each node located after a ReLU activation function. Their locations are visually depicted in Fig. 2. Then, we quantify the feature activation differences between the clean examples x and adversarial examples $x + \delta$ at selected activation nodes by

$$V_{act}^i(x, x + \delta) = \frac{1}{M} \sum_{x \in D_{train}} \|\mathcal{M}_i(x) - \mathcal{M}_i(x + \delta)\|_2, \quad (5)$$

where D_{train} is the training dataset and M is the number of samples in D_{train} . $\mathcal{M}_i(x)$ is features of x at the i -th activation node \mathcal{M}_i . $\|\cdot\|_2$ denotes the 2-norm function.

Fig. 1 shows the adversarial robustness of models and feature activation differences V_{act}^i per training epoch. In phases of stable adversarial training, $V_{act}^{A \sim C}$ converge to a

small value. However, they perform a sudden increase when models fall into CO. Furthermore, experimental results on various datasets and networks in supplementary materials exhibit similar phenomena.

Impact of δ to different channels. Now we know that CO is accompanied by salient feature activation differences. Next, we investigate if all or only several specific pathways show such differences. To determine this, we calculate channel-wise feature activation differences at \mathcal{M}_A on the test dataset D_{test} . We also conduct experiments on other nodes and show results in supplementary materials.

$$V_{act}^{i,k}(x, x + \delta) = \|\mathcal{M}_{i,k}(x) - \mathcal{M}_{i,k}(x + \delta)\|_2^2, \\ T_{act}^{i,k} = \tanh(\alpha \cdot \sum_{x \in D_{test}} \frac{V_{act}^{i,k}(x, x + \delta)}{N \cdot H \cdot W}), \quad (6)$$

where $\mathcal{M}_i(x) \in \mathbb{R}^{N \times H \times W}$, $\mathcal{M}_{i,k}$ denotes the k -th channel of \mathcal{M}_i , with $k \in [1, N]$. N , H and W correspond to the number of feature channels, the height and width of feature maps, respectively. $\|\cdot\|_2^2$ represents the squared 2-norm function. α is set to 100 for improved visualization.

Fig. 3 displays the channel-wise statistical information of $T_{act}^{A,k}$. The observations are as follows: 1) For models that suffer from CO, while most channels show a small $T_{act}^{A,k}$, a few channels exhibit significantly large values; 2) During stable adversarial training, $T_{act}^{A,k}$ of all channels tends to approach zero. Additionally, we find that the salient $T_{act}^{A,k}$ consistently occurs at the same channels across different adversarial examples. These findings suggest that adversarial perturbations mainly influence several specific pathways.

Exploring the role of different channels. Building upon the above experimental analyses, we propose an empirical hypothesis: channels with salient feature activation differences are primarily utilized to learn attack information. To verify this, we compare the classification performance of various masked models on both clean and adversarial examples. These models are obtained by masking diverse channels of a CO-affected model,

$$\mathcal{M}_{i,k}(x + \delta) \leftarrow 0 \quad \text{if } T_{act}^{i,k} > \alpha_2. \quad (7)$$

Based on statistic results of Fig. 3, we set the masking threshold α_2 to 1.0, 0.99, 0.5, and 0.1, respectively. Furthermore, the adversarial examples are generated against

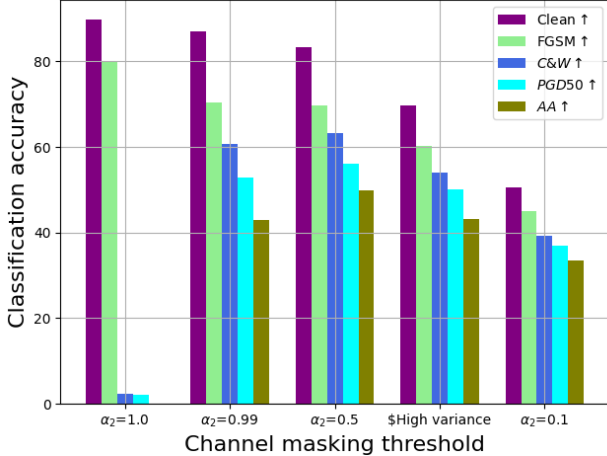


Figure 4. Classification accuracy of models suffering from CO on clean and adversarial examples under various channel masking thresholds. ‘ $\alpha_2=1.0$ ’ indicates the original classification accuracy. ‘\$High variance’ signifies using [18] to mask an equivalent number of channels as our method when ‘ $\alpha_2=0.5$ ’.

the original model ($\alpha_2 = 1.0$) using FGSM [14], PGD [26], C&W [5], and Autoattack (AA) [9]. They are directly used as inputs of masked models to evaluate. Fig. 4 shows the detailed evaluation results. (1) Masking the channels of $T_{act}^{A,k} > 0.99$ can efficiently improve the model performance on adversarial examples while only slightly affecting the performance on clean samples. (2) This trend continues when reducing α_2 to 0.5. (3) However, when α_2 is set to 0.1, the model performance on clean samples greatly decreases. These observations support our hypothesis. Notably, model channels cannot be directly divided into data or adversarial branches. This is because masking the pathways always influences the classification accuracy on clean samples.

Similarly, we provide the results of variance-based [18] channel masking in Fig. 4. Under an equal number of masked channels, the proposed activation difference shows superior prediction performance on both clean and adversarial data. This indicates the effectiveness of our approach in selecting pathways that extract attack information.

Overall, the misclassification of CO-affected models on adversarial examples can be attributed to feature coverage rather than feature destruction. Namely, adversarial perturbations do not greatly affect the extracted data information. Instead, they deceive models by increasing feature values of several specific channels. This explains why models can accurately recognize adversarial examples after removing the attack information based on Eq. (7).

3.2. Mitigating or inducing CO

Sec. 3.1 indicates that CO occurs with a significant increase of feature activation differences. We further validate this phenomenon by manipulating these differences to mitigate or induce CO. Specifically, to address CO, we introduce a

Nodes	α_3	Clean	FGSM	PGD-50	C&W	AA	CO
\mathcal{M}_A	100	64.95	40.41	25.9	20.38	16.91	✓
	200	57.28	36.12	24.35	20.01	16.84	✓
	400	10.00	10.00	10.00	10.00	10.00	–
	1000	10.00	10.00	10.00	10.00	10.00	–
\mathcal{M}_B	100	60.18	37.91	24.18	20.11	16.77	✓
	200	74.08	48.09	29.65	25.32	19.72	✗
	400	72.62	47.74	29.76	25.41	19.85	✗
	1000	71.30	46.89	29.73	25.53	20.97	✗
\mathcal{M}_C	100	54.45	34.76	24.43	20.06	17.32	✓
	200	58.11	37.57	25.69	20.49	17.16	✓
	400	63.66	38.11	24.30	18.71	15.59	✓
	1000	55.54	33.45	23.25	18.71	16.07	✓
\mathcal{M}_D	100	63.89	38.83	26.15	21.36	17.76	✓
	200	58.76	36.43	25.30	19.84	17.17	✓
	400	51.45	31.88	22.93	18.35	16.26	✓
	1000	44.86	30.32	24.12	20.35	18.55	✓
\mathcal{M}_E	100	49.72	32.83	24.03	22.47	19.87	✓
	200	54.55	34.97	25.68	22.39	19.68	✓
	400	55.20	36.67	26.48	22.67	19.94	✓
	1000	10.00	10.00	10.00	10.00	10.00	–

Table 1. Mitigating CO by suppressing feature differences at various activation nodes. $\xi_T = 12/255$ and $\xi_E = 16/255$. – means the failed convergence.

supplemental constraint for Eq. (1), which can suppress feature activation differences,

$$\mathcal{L}_{stable} = \frac{\alpha_3}{\mathbf{N} \cdot \mathbf{H} \cdot \mathbf{W}} \cdot \sum_k V_{act}^{i,k}(x + \delta, x + \delta_0), \quad (8)$$

where k denotes the k -th activation channel of the i -th activation node. α_3 can be assigned a large value since $V_{act}^{i,k}(x + \delta, x + \delta_0)$ converges towards zero under stable adversarial training. δ_0 and δ indicate the uniformly random perturbations and crafted adversarial perturbations, respectively. \mathcal{L}_{stable} establishes consistency between $\mathcal{M}_{i,k}(x + \delta)$ and $\mathcal{M}_{i,k}(x + \delta_0)$ rather than $\mathcal{M}_{i,k}(x)$. This reduces training time as $\mathcal{M}_{i,k}(x + \delta_0)$ is already calculated when generating adversarial perturbations δ .

The results in Tab. 1 show that only suppressing the feature activation differences at \mathcal{M}_B can resolve CO. In our opinion, this is due to \mathcal{M}_B being more sensitive to CO, as shown in Fig. 1. Tabs. 2 and 5 demonstrate that our approach achieves better or comparable performance than the state-of-the-art methods. Particularly, using the same hyperparameter ($\alpha_3 = 200$) can effectively mitigate CO across diverse datasets and networks. This alleviates the burden of hyperparameter selection in [48]. More detailed experimental analyses are given in supplementary materials.

Next, we explore how to induce CO. ξ_T is set to 8/255 since the adversarial training process is stable under this setting. $\xi_E = 16/255$. Sec. 3.1 shows that only several specific channels are responsible for CO. Thus, we first select the

Res-CIFAR10	ξ_T	Clean	PGD-50	C&W	AA	Mins	
<i>FGSM-MEP</i> [44]		74.71	35.52	33.05	27.23	92	
<i>C.Smooth</i> [48]		71.79	27.95	24.12	19.11	104	
<i>Ours</i>	$\alpha_3=100$	60.18	24.18	20.11	16.77	93	
	$\alpha_3=200$	$\frac{12}{255}$	74.08	29.65	25.32	19.72	93
	$\alpha_3=300$		73.13	29.36	25.06	19.58	93
	$\alpha_3=400$		72.62	29.76	25.41	19.85	93
	$\alpha_3=1000$		71.30	29.73	25.53	20.97	93
<i>FGSM-MEP</i> [44]		53.32	26.56	22.10	18.98	92	
<i>C.Smooth</i> [48]	$\frac{16}{255}$	63.84	32.95	28.19	23.68	104	
<i>Ours</i>	$\alpha_3=200$		65.01	34.17	29.79	22.85	93
Res-CIFAR100	ξ_T	Clean	PGD-50	C&W	AA	Mins	
<i>C.Smooth</i> [48]		50.61	14.70	12.54	9.04	104	
<i>Ours</i>	$\alpha_3=100$		51.27	14.81	12.71	9.82	93
	$\alpha_3=200$	$\frac{12}{255}$	51.01	14.86	13.06	10.08	93
	$\alpha_3=300$		50.51	14.87	12.69	9.83	93
	$\alpha_3=400$		50.44	14.49	12.41	9.64	93
	$\alpha_3=1000$		50.04	14.52	12.29	9.67	93
<i>C.Smooth</i> [48]	$\frac{16}{255}$	41.86	16.59	13.96	11.38	104	
<i>Ours</i>	$\alpha_3=200$		42.68	16.47	14.40	11.01	93

Table 2. Comparison with the state-of-the-art methods. ‘Res’ denotes the network ResNet18. The models are trained with perturbation budgets of 12/255 and 16/255, and evaluated with the perturbation budget of 16/255. ‘Mins’ is the minutes for training. Only the node \mathcal{M}_B is used to calculate \mathcal{L}_{stable} in Eq. (8).

feature channels with the top $p\%$ largest $T_{act}^{B,k}$ (denoted as $C_{p\%}$) based on the statistical information of training dataset. Then, we design the supplemental constraint for Eq. (1),

$$\mathcal{L}_{co} = \mathcal{L}(\mathcal{M}(x + \delta, C_{p\%}), y) - \mathcal{L}_{stable}(C_{p\%}), \quad (9)$$

where $\mathcal{M}(\cdot, C_{p\%})$ denotes the models masked $C_{p\%}$. The former item ensures that the masked models can correctly classify adversarial examples, and the latter enlarges the feature differences of channels $k \in C_{p\%}$. p is set to 1, 3, 10, and 20 respectively. As depicted in Fig. 5, \mathcal{L}_{co} with $C_{10\%}$ can bring about CO. Moreover, adding \mathcal{L}_{co} to $C_{1\%}$ is insufficient to induce CO, whereas introducing \mathcal{L}_{co} to $C_{20\%}$ prevents the model from converging. Furthermore, we conduct a comparative experiment based on [18] by selecting feature channels with the top 10% maximum channel variance. Fig. 6 shows that the model is difficult to converge under this setting. In our opinion, this is because several selected channels mainly capture data information, and increasing their variance affects the model optimization.

4. Leveraging CO to enhance performance

In the preceding section, we have discussed the underlying causes of CO and its potential solutions. Drawing from these insights, we then illustrate whether CO has to be solved. Specifically, we try to improve the performance of

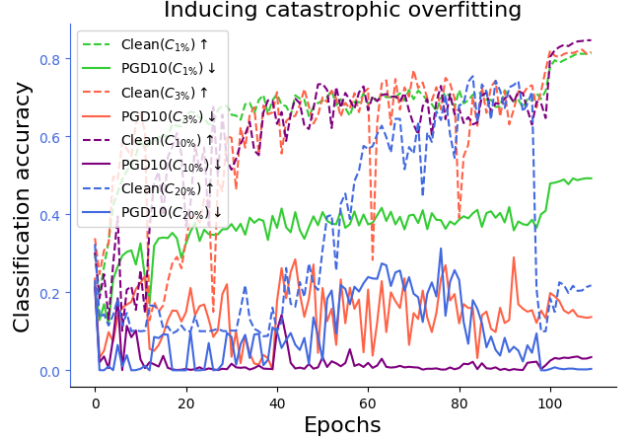


Figure 5. Investigate whether \mathcal{L}_{co} in Eq. (9) can induce CO.

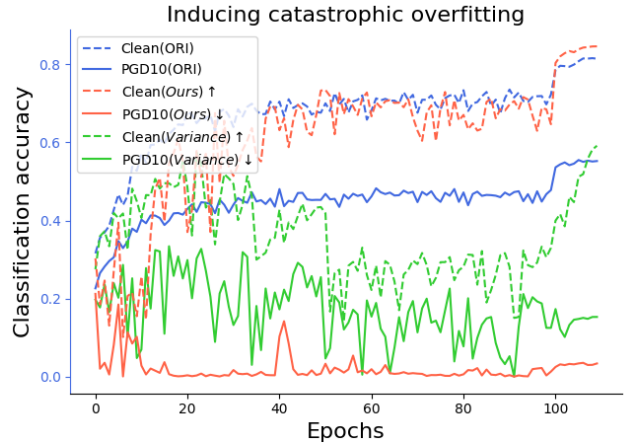


Figure 6. Comparison with prior work [18] in inducing CO.

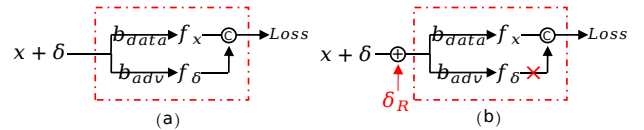


Figure 7. The structure of models that suffer from CO. (a) Original structure; (b) The structure of adding random noise δ_R . f denotes the extracted features.

CO-affected models by leveraging their different pathways for extracting data and attack information. Although these pathways are not entirely separable, we describe them as two distinct branches in Fig. 7 (a) for clarity, *i.e.*, the data branch ‘ b_{data} ’ and the adversarial branch ‘ b_{adv} ’.

4.1. Attack obfuscation

We expect that adversarial attacks mainly deceive the branch b_{adv} and that the models primarily use features extracted from the branch b_{data} to classify both clean and adversarial examples, which is called attack obfuscation. Fortunately, models that suffer from CO inherently satisfy the former expectation, as shown in Fig. 3 and Fig. 4. The lat-

	<i>Origin</i>	<i>CO.</i>	<i>Stable</i>
w/o. δ_R	94.40	89.81	72.84
w. δ_R	80.63	89.64	72.06

Table 3. Classification accuracy of various models on clean samples. ‘*Origin*’ denotes the performance of the original ResNet18. ‘*Stable*’ represents the stably trained model. ‘*CO.*’ means the model suffering from catastrophic overfitting. $\xi_T = 12/255$ and $\delta_R \sim U(-16/255, 16/255)$. $U(\cdot, \cdot)$ is uniformly random noise.

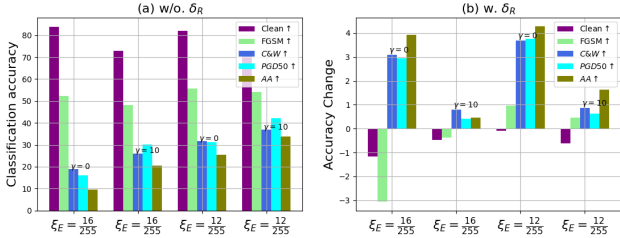


Figure 8. Relationship between adversarial robustness and capacity of withstanding noise interference for adversarial perturbations. $\xi_T = 12/255$. ξ_E is set to 12/255 or 16/255. (a) Classification accuracy of models. (b) The degree of change in classification accuracy when adding uniformly random noise $\delta_R \sim U(-16/255, 16/255)$.

ter contains twofold: 1) the model performance in regular tasks should be preserved; 2) the attack information carried by adversarial perturbations can be disrupted. These can be realized by introducing random noise δ_R to the input of CO-affected models during inference, as shown in Fig. 7 (b). To explain this, we take the uniformly random noise ($\delta_R \sim U(-16/255, 16/255)$) as an example. In the following, δ_0 , δ , and δ_R represent the initial adversarial perturbation, the crafted adversarial perturbation, and the random noise added to model input, respectively.

It can be observed in Tab. 3 that the model suffering from CO displays well generalization to δ_R . Meanwhile, we find in Fig. 9 that adversarial perturbations for deceiving CO-affected models maintain the limited attack ability after adding δ_R . This is a common phenomenon because: 1) Compared to stably trained models, CO-affected models show a significant decrease in adversarial robustness; 2) As the adversarial robustness of victim models decreases, the capacity of withstanding noise interference weakens for adversarial perturbations. To validate this, we train two comparative models with $\xi_T = 12/255$. The distinction between them is whether using the regularization term in [44],

$$\gamma \cdot \|\mathcal{M}(x + \delta) - \mathcal{M}(x + \delta_0)\|_2^2. \quad (10)$$

The adversarial examples for evaluation are generated under two perturbation budgets: 12/255 and 16/255. Fig. 8 (a) shows that Eq. (10) can greatly improve the adversarial robustness of models. Furthermore, Fig. 8 (b) indicates that adding random noise δ_R has the limited influence on the models with strong adversarial robustness.

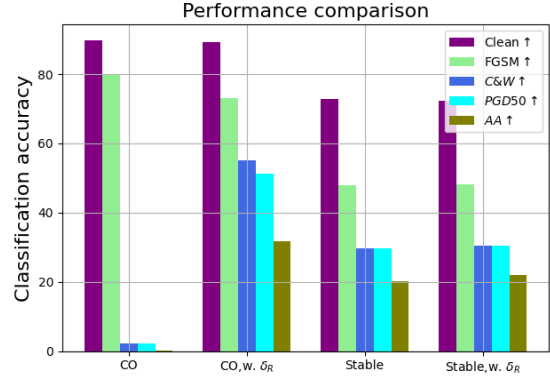


Figure 9. Classification accuracy of various models on clean and adversarial data. $\xi_T = 12/255$, $\xi_E = 16/255$, and $\delta_R \sim U(-16/255, 16/255)$. $U(\cdot, \cdot)$ is uniformly random noise.

$U(-a, a)$	<i>Gauss</i> (σ)	<i>Clean</i>	<i>PGD-50</i>	<i>C&W</i>	<i>AA</i>
$a = 10/255$	-	88.26	33.85	38.90	23.27
$a = 12/255$	-	88.44	46.49	50.01	33.70
$a = 14/255$	-	88.39	54.07	58.03	40.56
$a = 16/255$	-	88.45	58.48	61.65	43.53
-	10/255	87.80	54.25	58.14	39.73
-	12/255	86.41	56.74	60.22	41.64
-	14/255	83.84	57.26	59.74	41.48
-	16/255	80.25	55.81	58.68	40.34

Table 4. Ablation studies for types of random noise δ_R on the robustness of CO-affected models. Experiments are conducted on CIFAR10 with ResNet18. $U(\cdot, \cdot)$ is uniformly random noise, while *Gauss* denotes Gaussian noise with an average of 0. σ is the standard deviation of *Gauss*.

Performance comparison of various models. In Tab. 3, CO-affected models exhibit higher classification accuracy on clean samples (89.81%) than stably trained models (72.84%). Furthermore, they display excellent generalization performance to noise-perturbed examples, achieving an accuracy of 89.64%. Additionally, experimental results in Fig. 9 and Tab. 5 show that adding uniformly random noise to the input of CO-affected models can attain the optimal adversarial robustness. In summary, CO can be utilized to enhance the model performance on both clean and adversarial examples. Experiments on various datasets and networks in supplementary materials also support this conclusion.

Ablation studies on types of random noise δ_R . In addition to applying uniformly random noise, we also explore the impact of Gaussian noise on the performance of CO-affected models ($\xi_T = 16/255$). For Gaussian noise, we vary the standard deviation with values of 10/255, 12/255, 14/255, and 16/255, keeping the mean value at 0. The experimental results are shown in Tab. 4. It can be observed that adding $\delta_R \sim U(-16/255, 16/255)$ to model inputs achieves the optimal classification accuracy on both clean and adversarial data. More results about models under various ξ_T can be found in supplementary materials.

ξ_T	Methods	Clean \uparrow	FGSM \uparrow	PGD-10 \uparrow	PGD-20 \uparrow	PGD-50 \uparrow	C&W \uparrow	APGD-T[9] \uparrow	AA \uparrow
10/255	ATAS [19]	83.43	48.09	31.29	19.43	15.37	18.55	12.93	10.94
	ZeroGrad [13]	82.70	45.32	30.26	18.59	14.93	17.59	12.47	10.97
	C.Smooth [48]	76.10	47.12	37.30	28.16	26.11	23.48	19.32	18.23
	Ours-FD.	76.73	48.85	39.59	30.82	28.61	26.58	21.91	20.07
	Ours-CO.	88.91	70.07	58.45	48.04	38.63	49.41	41.31	19.45
12/255	ATAS [19]	83.52	49.02	33.25	21.78	17.73	21.15	14.06	11.91
	ZeroGrad [13]	82.17	48.98	33.81	22.37	18.34	21.65	14.98	12.85
	C.Smooth [48]	71.79	45.73	37.79	29.81	27.95	24.12	19.71	19.11
	Ours-FD.	72.60	49.08	40.87	33.06	31.42	28.16	23.33	22.08
	Ours-CO.	89.39	73.18	64.15	57.32	51.25	58.82	55.13	31.62
14/255	ATAS [19]	81.54	48.96	34.24	23.05	19.54	21.91	15.69	13.38
	ZeroGrad [13]	74.23	46.76	35.42	25.27	21.94	23.19	18.03	15.64
	C.Smooth [48]	65.57	45.40	38.75	32.33	31.20	25.97	23.15	22.51
	Ours-FD.	68.98	47.67	40.55	33.96	32.56	28.10	24.36	23.54
	Ours-CO.	89.12	71.48	61.46	53.72	46.29	54.29	56.01	30.65
16/255	ATAS [19]	79.91	52.28	38.96	28.64	25.16	27.83	23.82	16.95
	ZeroGrad [13]	67.34	42.07	32.46	25.35	22.45	21.33	15.79	15.15
	C.Smooth [48]	62.88	44.98	40.98	35.48	34.29	29.94	26.23	25.10
	Ours-FD.	64.08	48.02	42.56	37.43	36.83	32.51	28.62	27.37
	Ours-CO.	88.45	71.59	66.27	60.59	58.48	61.65	62.03	43.53

Table 5. Quantitative results of various FAT methods when adding $\delta_R \sim U(-16/255, 16/255)$ to inputs. We adopt ResNet18 and CIFAR-10. $U(\cdot, \cdot)$ is uniformly random noise. Models are evaluated with $\xi_E = 16/255$. Our methods employ the same baseline as [48]. For ATAS and ZeroGrad, we employ the early stopping technique [36] when these methods falling into CO. *FD* means the proposed feature difference.

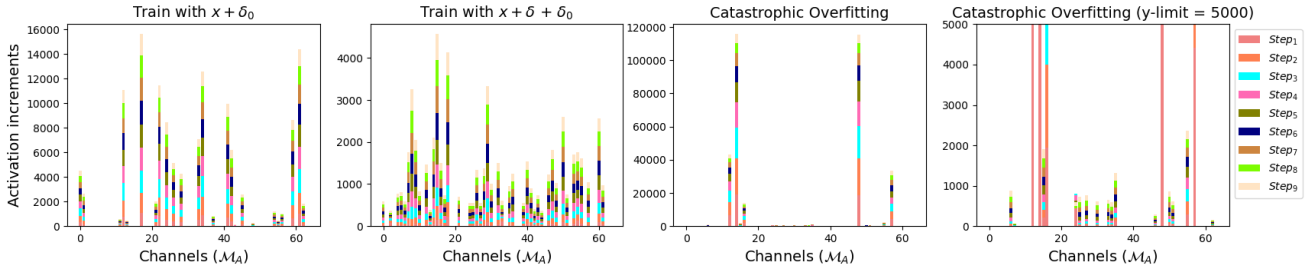


Figure 10. Activation increments observed in various models at each step of the PGD-10 attack. We statistic the results within the test set. $Step_i$ is activation increments induced by the i -th adversarial attack. δ and δ_0 denote adversarial and random perturbations, respectively.

4.2. Necessity of inducing CO for robustness

We believe that the robustness improvement of CO-affected models is not solely ascribed to their generalization ability to noise. To verify this, we conduct comparative experiments by utilizing various noise-augmented data to train models. We first augment training data by adding uniformly random noise δ_0 , with $\xi_T = 16/255$,

$$\min_{\theta} \mathbb{E}_{(x,y) \sim D_{train}} [\mathcal{L}(\mathcal{M}(x + \delta_0), y)]. \quad (11)$$

As depicted in Fig. 11 (a), the effective generalization to δ_0 does not improve adversarial robustness.

We then assess the augmentation strategy of superposing adversarial perturbation δ and uniformly random noise δ_0 .

$$\min_{\theta} \mathbb{E}_{(x,y) \sim D_{train}} [\mathcal{L}(\mathcal{M}(x + \delta + \delta_0), y)]. \quad (12)$$

In Fig. 11 (a), the generalization to $\delta + \delta_0$ helps improve the adversarial robustness. However, this benefit is con-

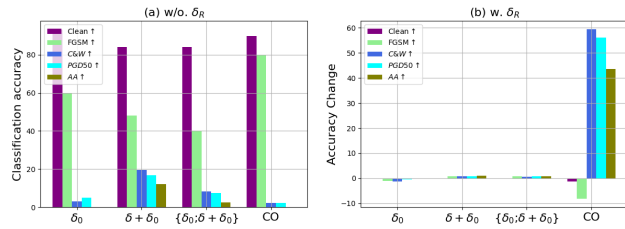


Figure 11. Comparative experiments on models trained with various noise-augmented data. (a) Classification accuracy of initial models. (b) The degree of change in classification accuracy when adding $\delta_R \sim U(-16/255, 16/255)$ to model inputs. δ_0 : augment training data by adding random noise. $\delta + \delta_0$: superposing adversarial perturbation and random noise. $\{\delta; \delta + \delta_0\}$: combining the noise-augmented data $x + \delta_0$ and $x + \delta + \delta_0$.

siderably lower than that of adding δ_R to the input of CO-affected models, as shown in Fig. 11 (b). It is also evident that utilizing both $x + \delta_0$ and $x + \delta + \delta_0$ as training data does not result in stronger adversarial robustness.

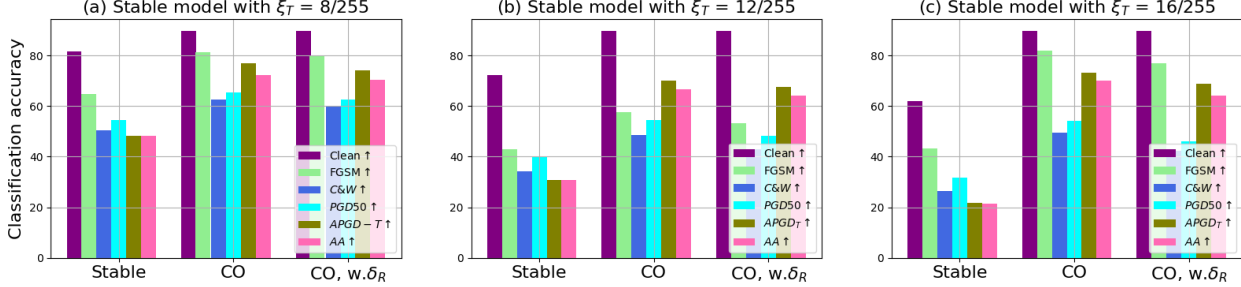


Figure 12. Classification accuracy of CO-affected models ($\xi_T = 12/255$) for transferred adversarial examples. Experiments are studied on CIFAR-10 with ResNet18. (a) $\xi_E = 8/255$; (b) $\xi_E = 12/255$; (c) $\xi_E = 16/255$. $\delta_R \sim U(-16/255, 16/255)$. $U(\cdot, \cdot)$ is uniformly random noise.

To understand the differences between CO-affected and noise-augmented models, we display channel-specific activation increments $\sum_{x \in D_{test}} \frac{V_{act}^{i,k}(x, x + \delta_j)}{N \cdot H \cdot W}$ at each step j of adversarial attacks in Fig. 10. Comparatively, CO-affected models exhibit salient activation increments in several specific channels, while noise-augmented models show comparable activation increments across different channels. Hence, we think that for noise-augmented models, the channels responsible for learning data and attack information are nearly inseparable. Consequently, adversarial attacks on these models are more likely to affect the channels of learning data information. For instance, many activation increments in noise-augmented models surpass 1000, exceeding the levels observed in CO-affected models. These findings, coupled with the performance comparison between CO-affected and noise-augmented models in Fig. 11, indirectly validate the fact of ‘attack obfuscation’.

Crucially, for the models trained on clean samples, adding uniformly random noise to their input does not improve the adversarial robustness. The experimental results are shown in Tab. 6. It can be seen that these models are not robust against adversarial attacks such as PGD and C&W.

4.3. Robustness against transferred $x + \delta$

We explore the performance of CO-affected models when they are exposed to transferred adversarial examples. Specifically, we initially train stable models using [48] under perturbation budgets of 8/255, 12/255, and 16/255, respectively. Subsequently, we generate adversarial examples against these stable models and evaluate the attack performance of these examples on a CO-affected model ($\xi_T = 12/255$). The results on CIFAR10 are provided in Fig. 12, which demonstrate the weak attack performance of these adversarial examples. Additionally, we find a similar phenomenon on CIFAR100 in supplementary materials.

4.4. Various FAT baselines

In previous sections, we primarily utilize the FGSM-MEP as the FAT baseline. Here, we conduct experiments based on FGSM-RS [41]. It can be observed from Tab. 7 that

Res-CIFAR10	Clean	FGSM	PGD-50	C&W	AA
w/o. δ_R	94.40	2.13	0.00	0.00	0.00
w. δ_R	80.63	4.07	0.00	0.00	0.00
Res-CIFAR100	Clean	FGSM	PGD-50	C&W	AA
w/o. δ_R	76.64	1.31	0.00	0.00	0.00
w. δ_R	47.53	3.02	0.00	0.00	0.00

Table 6. Classification accuracy of models trained on clean samples. ‘Res’ denotes the network ResNet18. $\delta_R \sim U(-16/255, 16/255)$. $U(\cdot, \cdot)$ denotes the uniformly random noise.

ξ_T	$\delta_R \sim U(-a, a)$	Clean	PGD-50	C&W	AA
10/255	a = 0.	79.97	2.66	4.15	0.00
	a = 16/255	85.84	38.99	44.00	25.85
12/255	a = 0.	85.10	0.50	0.51	0.00
	a = 16/255	86.58	39.25	45.72	26.03
14/255	a = 0.	82.81	0.14	0.39	0.00
	a = 16/255	87.59	44.99	52.76	24.55
16/255	a = 0.	70.97	0.16	0.29	0.00
	a = 16/255	85.75	46.55	53.29	26.89

Table 7. Classification accuracy of models trained by [41]. We adopt the dataset CIFAR10 and the network ResNet18. $U(\cdot, \cdot)$ denotes the uniformly random noise.

applying random noise $\delta_R + \delta$ to the model trained by FGSM-RS also significantly improves its adversarial robustness.

5. Conclusion

In this work, we provide a comprehensive explanation for CO by analyzing the feature activation differences between clean and adversarial examples. Our studies reveal that CO occurs with salient feature activation differences. On this basis, we propose novel regularization terms to either mitigate or induce CO by manipulating feature differences, which indirectly validates the relationship between CO and these differences. Importantly, our regularization terms are insensitive to hyperparameters. Furthermore, we incorporate random noise into CO-affected models, thereby achieving optimal classification accuracy for both clean and adversarial examples. To explain this phenomenon, we approach it from the perspective of attack obfuscation.

References

- [1] Sravanti Addepalli, Samyak Jain, Gaurang Sriramanan, and R Venkatesh Babu. Scaling adversarial training to large perturbation bounds. In *European Conference on Computer Vision*, pages 301–316. Springer, 2022. [3](#)
- [2] Flammarion N Andriushchenko M. Understanding and improving fast adversarial training. In *Advances in Neural Information Processing Systems*, pages 16048–16059, 2020. [1](#)
- [3] Vadim Borisov, Tobias Leemann, Kathrin Seßler, Johannes Haug, Martin Pawelczyk, and Gjergji Kasneci. Deep neural networks and tabular data: A survey. *IEEE Transactions on Neural Networks and Learning Systems*, 2022. [1](#)
- [4] Yulong Cao, Chaowei Xiao, Anima Anandkumar, Danfei Xu, and Marco Pavone. Advdo: Realistic adversarial attacks for trajectory prediction. In *European Conference on Computer Vision*, pages 36–52. Springer, 2022. [1](#)
- [5] Nicholas Carlini and David Wagner. Towards evaluating the robustness of neural networks. In *IEEE Symposium on Security and Privacy*, pages 39–57, 2017. [4](#)
- [6] Weixin Chen, Baoyuan Wu, and Haoqian Wang. Effective backdoor defense by exploiting sensitivity of poisoned samples. *Advances in Neural Information Processing Systems*, 35:9727–9737, 2022. [1](#)
- [7] Yaya Cheng, Jingkuan Song, Xiaosu Zhu, Qilong Zhang, Lianli Gao, and Heng Tao Shen. Fast gradient non-sign methods. *arXiv preprint arXiv:2110.12734*, 2021. [2](#)
- [8] Sheng-Yen Chou, Pin-Yu Chen, and Tsung-Yi Ho. How to backdoor diffusion models? In *Proceedings of the IEEE/CVF Conference on Computer Vision and Pattern Recognition*, pages 4015–4024, 2023. [1](#)
- [9] Francesco Croce and Matthias Hein. Reliable evaluation of adversarial robustness with an ensemble of diverse parameter-free attacks. In *International Conference on Machine Learning*, 2020. [4](#), [7](#)
- [10] Pau de Jorge Aranda, Adel Bibi, Riccardo Volpi, Amartya Sanyal, Philip Torr, Grégory Rogez, and Puneet Dokania. Make some noise: Reliable and efficient single-step adversarial training. *Advances in Neural Information Processing Systems*, 35:12881–12893, 2022. [1](#)
- [11] Yinpeng Dong, Fangzhou Liao, Tianyu Pang, Hang Su, Jun Zhu, Xiaolin Hu, and Jianguo Li. Boosting adversarial attacks with momentum. In *Proceedings of the IEEE conference on computer vision and pattern recognition*, pages 9185–9193, 2018. [2](#)
- [12] Z. Golgooni, M. Saberi, M. Eskandar, and M. H Rohban. Zerograd: Mitigating and explaining catastrophic overfitting in fgsm adversarial training. page arXiv preprint arXiv:2103.15476, 2021. [2](#)
- [13] Zeinab Golgooni, Mehrdad Saberi, Masih Eskandar, and Mohammad Hossein Rohban. Zerograd: Costless conscious remedies for catastrophic overfitting in the fgsm adversarial training. *Intelligent Systems with Applications*, 19:200258, 2023. [7](#)
- [14] Ian J Goodfellow, Jonathon Shlens, and Christian Szegedy. Explaining and harnessing adversarial examples. In *International Conference on Learning Representations (ICLR)*, 2015. [1](#), [2](#), [4](#)
- [15] Jindong Gu, Hengshuang Zhao, Volker Tresp, and Philip HS Torr. Segpgd: An effective and efficient adversarial attack for evaluating and boosting segmentation robustness. In *European Conference on Computer Vision*, pages 308–325. Springer, 2022. [1](#)
- [16] Luis Guzman-Nateras, Minh Van Nguyen, and Thien Nguyen. Cross-lingual event detection via optimized adversarial training. In *Proceedings of the 2022 Conference of the North American Chapter of the Association for Computational Linguistics: Human Language Technologies*, pages 5588–5599, 2022. [1](#)
- [17] Kaiming He, Xiangyu Zhang, Shaoqing Ren, and Jian Sun. Deep residual learning for image recognition. In *Proceedings of the IEEE conference on computer vision and pattern recognition*, pages 770–778, 2016. [1](#)
- [18] Zhengbao He, Tao Li, Sizhe Chen, and Xiaolin Huang. Investigating catastrophic overfitting in fast adversarial training: A self-fitting perspective. In *Proceedings of the IEEE/CVF Conference on Computer Vision and Pattern Recognition*, pages 2313–2320, 2023. [1](#), [2](#), [3](#), [4](#), [5](#)
- [19] Zhichao Huang, Yanbo Fan, Chen Liu, Weizhong Zhang, Yong Zhang, Mathieu Salzmann, Sabine Süsstrunk, and Jue Wang. Fast adversarial training with adaptive step size. *arXiv preprint arXiv:2206.02417*, 2022. [1](#), [7](#)
- [20] Xiaojun Jia, Yong Zhang, Baoyuan Wu, Ke Ma, Jue Wang, and Xiaochun Cao. Las-at: adversarial training with learnable attack strategy. In *Proceedings of the IEEE/CVF Conference on Computer Vision and Pattern Recognition*, pages 13398–13408, 2022. [1](#)
- [21] Xiaojun Jia, Yong Zhang, Baoyuan Wu, Jue Wang, and Xiaochun Cao. Boosting fast adversarial training with learnable adversarial initialization. *IEEE Transactions on Image Processing*, 31:4417–4430, 2022. [1](#), [2](#)
- [22] Gaojie Jin, Xinpeng Yi, Wei Huang, Sven Schewe, and Xiao-wei Huang. Enhancing adversarial training with second-order statistics of weights. In *Proceedings of the IEEE/CVF Conference on Computer Vision and Pattern Recognition*, pages 15273–15283, 2022. [1](#), [2](#)
- [23] Alex Krizhevsky, Geoffrey Hinton, et al. Learning multiple layers of features from tiny images. 2009. [1](#)
- [24] A. Kurakin, I.J. Goodfellow, and S. Bengio. Adversarial machine learning at scale. In *International Conference on Learning Representations (ICLR)*, 2017. [2](#)
- [25] Tao Li, Yingwen Wu, Sizhe Chen, Kun Fang, and Xiaolin Huang. Subspace adversarial training. In *Proceedings of the IEEE/CVF Conference on Computer Vision and Pattern Recognition*, pages 13409–13418, 2022. [1](#)
- [26] Aleksander Madry, Aleksandar Makelov, Ludwig Schmidt, Dimitris Tsipras, and Adrian Vladu. Towards deep learning models resistant to adversarial attacks. In *International Conference on Learning Representations (ICLR)*, 2018. [1](#), [2](#), [4](#)
- [27] Yichuan Mo, Dongxian Wu, Yifei Wang, Yiwen Guo, and Yisen Wang. When adversarial training meets vision transformers: Recipes from training to architecture. *Advances in Neural Information Processing Systems*, 35:18599–18611, 2022. [1](#)
- [28] S Mostafa Mousavi and Gregory C Beroza. Deep-learning seismology. *Science*, 377(6607):eabm4470, 2022. [1](#)

- [29] Axi Niu, Kang Zhang, Chaoning Zhang, Chenshuang Zhang, In So Kweon, Chang D Yoo, and Yanning Zhang. Fast adversarial training with noise augmentation: A unified perspective on randstart and gradalign. *arXiv preprint arXiv:2202.05488*, 2022. [2](#)
- [30] Nicolas Papernot, Patrick McDaniel, Somesh Jha, Matt Fredrikson, Z Berkay Celik, and Ananthram Swami. The limitations of deep learning in adversarial settings. In *2016 IEEE European symposium on security and privacy (EuroS&P)*, pages 372–387. IEEE, 2016. [2](#)
- [31] Geon Yeong Park and Sang Wan Lee. Reliably fast adversarial training via latent adversarial perturbation. In *Proceedings of the IEEE/CVF International Conference on Computer Vision*, pages 7758–7767, 2021. [2](#)
- [32] Talmo D Pereira, Nathaniel Tabris, Arie Matsliah, David M Turner, Junyu Li, Shruthi Ravindranath, Eleni S Papadoyannis, Edna Normand, David S Deutsch, Z Yan Wang, et al. Slep: A deep learning system for multi-animal pose tracking. *Nature methods*, 19(4):486–495, 2022. [1](#)
- [33] Leslie Rice, Eric Wong, and Zico Kolter. Overfitting in adversarially robust deep learning. In *International Conference on Machine Learning*, pages 8093–8104. PMLR, 2020. [1](#)
- [34] Zohaib Salahuddin, Henry C Woodruff, Avishek Chatterjee, and Philippe Lambin. Transparency of deep neural networks for medical image analysis: A review of interpretability methods. *Computers in biology and medicine*, 140:105111, 2022. [1](#)
- [35] Ali Shafahi, Mahyar Najibi, Mohammad Amin Ghiasi, Zheng Xu, John Dickerson, Christoph Studer, Larry S Davis, Gavin Taylor, and Tom Goldstein. Adversarial training for free! *Advances in Neural Information Processing Systems*, 32, 2019. [2](#)
- [36] Chawin Sitawarin, Supriyo Chakraborty, and David Wagner. Sat: Improving adversarial training via curriculum-based loss smoothing. In *Proceedings of the 14th ACM Workshop on Artificial Intelligence and Security*, pages 25–36, 2021. [7](#)
- [37] Gaurang Sriramanan, Sravanti Addepalli, Arya Baburaj, et al. Towards efficient and effective adversarial training. pages 11821–11833, 2021. [2](#)
- [38] Florian Tramer and Dan Boneh. Adversarial training and robustness for multiple perturbations. *Advances in neural information processing systems*, 32, 2019. [2](#)
- [39] Chen Wan, Fangjun Huang, and Xianfeng Zhao. Average gradient-based adversarial attack. *IEEE Transactions on Multimedia*, 2023. [2](#)
- [40] Lin Wei, Long Jin, and Xin Luo. Noise-suppressing neural dynamics for time-dependent constrained nonlinear optimization with applications. *IEEE Transactions on Systems, Man, and Cybernetics: Systems*, 52(10):6139–6150, 2022. [1](#)
- [41] Kolter J Z, Wong E, Rice L. Fast is better than free: Revisiting adversarial training. In *International Conference on Learning Representations (ICLR)*, 2020. [1](#), [2](#), [8](#)
- [42] Boxi Wu, Jindong Gu, Zhifeng Li, Deng Cai, Xiaofei He, and Wei Liu. Towards efficient adversarial training on vision transformers. In *European Conference on Computer Vision*, pages 307–325. Springer, 2022. [1](#), [2](#)
- [43] Jiancong Xiao, Yanbo Fan, Ruoyu Sun, Jue Wang, and Zhi-Quan Luo. Stability analysis and generalization bounds of adversarial training. *Advances in Neural Information Processing Systems*, 35:15446–15459, 2022. [1](#)
- [44] Jia Xiaojun, Zhang Yong, Wei Xingxing, Wu Baoyuan, Ma Ke, Wang Jue, and Cao Xiaochun. Prior-guided adversarial initialization for fast adversarial training. In *Proceedings of the European conference on computer vision (ECCV)*, 2022. [1](#), [3](#), [5](#), [6](#)
- [45] Zheng Yuan, Jie Zhang, Yunpei Jia, Chuanqi Tan, Tao Xue, and Shiguang Shan. Meta gradient adversarial attack. In *Proceedings of the IEEE/CVF International Conference on Computer Vision*, pages 7748–7757, 2021. [2](#)
- [46] Hongyang Zhang, Yaodong Yu, Jiantao Jiao, Eric Xing, Laurent El Ghaoui, and Michael Jordan. Theoretically principled trade-off between robustness and accuracy. In *International conference on machine learning*, pages 7472–7482. PMLR, 2019. [2](#)
- [47] Yihua Zhang, Guanhua Zhang, Prashant Khanduri, Mingyi Hong, Shiyu Chang, and Sijia Liu. Revisiting and advancing fast adversarial training through the lens of bi-level optimization. In *International Conference on Machine Learning*, pages 26693–26712. PMLR, 2022. [1](#)
- [48] Mengnan Zhao, Lihe Zhang, Yuqiu Kong, and Baocai Yin. Fast adversarial training with smooth convergence. In *Proceedings of the IEEE/CVF International Conference on Computer Vision*, pages 4720–4729, 2023. [1](#), [2](#), [3](#), [4](#), [5](#), [7](#), [8](#)
- [49] Yiqi Zhong, Xianming Liu, Deming Zhai, Junjun Jiang, and Xiangyang Ji. Shadows can be dangerous: Stealthy and effective physical-world adversarial attack by natural phenomenon. In *Proceedings of the IEEE/CVF Conference on Computer Vision and Pattern Recognition*, pages 15345–15354, 2022. [1](#)
- [50] Chao Zuo, Jiaming Qian, Shijie Feng, Wei Yin, Yixuan Li, Pengfei Fan, Jing Han, Kemao Qian, and Qian Chen. Deep learning in optical metrology: a review. *Light: Science & Applications*, 11(1):39, 2022. [1](#)